International Journal of Chemical, Materials and Biomolecular Sciences
ISSN: 2415-6620
Vol:10, No:4, 2016

Modeling Aerosol Formation in an Electrically Heated Tobacco Product

Markus Nordlund, Arkadiusz K. Kuczaj

Abstract—Philip Morris International (PMI) is developing a range of novel tobacco products with the potential to reduce individual risk and population harm in comparison to smoking cigarettes. One of these products is the Tobacco Heating System 2.2 (THS 2.2), (named as the Electrically Heated Tobacco System (EHTS) in this paper), already commercialized in a number of countries (e.g., Japan, Italy, Switzerland, Russia, Portugal and Romania). During use, the patented EHTS heats a specifically designed tobacco product (Electrically Heated Tobacco Product (EHTP)) when inserted into a Holder (heating device). The EHTP contains tobacco material in the form of a porous plug that undergoes a controlled heating process to release chemical compounds into vapors, from which an aerosol is formed during cooling. The aim of this work was to investigate the aerosol formation characteristics for realistic operating conditions of the EHTS as well as for relevant gas mixture compositions measured in the EHTP aerosol consisting mostly of *water*, *glycerol* and *nicotine*, but also other compounds at much lower concentrations. The nucleation process taking place in the EHTP during use when operated in the Holder has therefore been modeled numerically using an extended Classical Nucleation Theory (CNT) for multicomponent gas mixtures. Results from the performed simulations demonstrate that aerosol droplets are formed only in the presence of an aerosol former being mainly *glycerol*. Minor compounds in the gas mixture were not able to reach a supersaturated state alone and therefore could not generate aerosol droplets from the multicomponent gas mixture at the operating conditions simulated. For the analytically characterized aerosol composition and estimated operating conditions of the EHTS and EHTP, *glycerol* was shown to be the main aerosol former triggering the nucleation process in the EHTP. This implies that according to the CNT, an aerosol former, such as *glycerol* needs to be present in the gas mixture for an aerosol to form under the tested operating conditions. To assess if these conclusions are sensitive to the initial amount of the minor compounds and to include and represent the total mass of the aerosol collected during the analytical aerosol characterization, simulations were carried out with initial masses of the minor compounds increased by as much as a factor of 500. Despite this extreme condition, no aerosol droplets were generated when *glycerol*, *nicotine* and *water* were treated as inert species and therefore not actively contributing to the nucleation process. This implies that according to the CNT, an aerosol cannot be generated without the help of an aerosol former, from the multicomponent gas mixtures at the compositions and operating conditions estimated for the EHTP, even if all minor compounds are released or generated in a single puff.

Keywords—Aerosol, Classical Nucleation Theory (CNT), Electrically Heated Tobacco Product (EHTP), Electrically Heated Tobacco System (EHTS), modeling, multicomponent, nucleation.

M. Nordlund is employed by Philip Morris International Research & Development, Philip Morris Products S.A., Quai Jeanrenaud 5, CH-2000 Neuchâtel, Switzerland (e-mail: markus.nordlund@pmi.com).

A.K. Kuczaj is with the Multiscale Modeling & Simulation, Dept. of Applied Mathematics, University of Twente, P.O. Box 217, 7500 AE Enschede, The Netherlands and also employed by Philip Morris International Research & Development, Philip Morris Products S.A., Quai Jeanrenaud 5, CH-2000 Neuchâtel, Switzerland.

I. Introduction

DURING the use of the EHTP when operated in the Holder, gaseous compounds are released from the heated tobacco. This implies that the aerosol formation in an EHTP is formed from a multicomponent gas mixture, of over hundreds of chemical compounds. The aerosol droplets are formed when the multicomponent gas mixture constituents reach their supersaturated states when being subject to rapid cooling when air is drawn through the EHTP during puffing. This process and the dynamics of an aerosol forming from a gaseous mixture of various chemical species is expressed by the detailed interplay between nucleation, evaporation and condensation, as well as coalescence, interacting with vapor concentration, temperature, pressure and velocity fields [1]. Moreover, the aerosol generation and evolution are strongly dependent on the temperature dependent thermophysical properties of the individual compounds constituting the multicomponent gas mixture and the resulting mixture composition and properties. The aerosol generation process is very challenging to measure experimentally even for single component aerosols with large experimental variations reported in literature [2]–[4]. This is especially true for complex multicomponent aerosols [5]. An alternative method to determine the aerosol generation is to use coupled models of the nucleation, condensation, evaporation and coagulation processes that can be integrated into a computational framework, which can numerically be solved to predict aerosol nucleation, aerosol droplet composition and sizes, etc. [6], [7].

In this work, the focus is on modeling the aerosol generation by nucleation of a supersaturated multicomponent gas mixture composed of compounds measured in the EHTP aerosol. The supersaturated gas mixture is exposed to rapid cooling conditions representative of the operating conditions in the Holder during use. The approach taken in this work is that of an extended CNT for multicomponent aerosol mixtures. The extended model closely follows the approach of [8], [9], allowing for the approximation of aerosol properties in multicomponent systems up to hundreds of compounds. It was shown by [10] that the extended CNT was capable of determining the nucleation process for multicomponent alcohol gas mixtures for a ternary system of alcohol vapors with less computational effort than the more elaborated Becker-Döring theory [11]. In this work, the models for nucleation, condensation and coagulation were implemented into a Segregated, Finite-Volume (FV) based Computational Fluid Dynamics (CFD) code using the Open source Field Operations and Manipulations (OpenFOAM®)

software package [12], [13]. The robustness and accuracy of the extended Pressure-Implicit with Splitting of Operators (PISO) algorithm for aerosol dynamics were rigorously tested and validated for single component aerosol formation in [6], [7].

In this work, various simulation cases were considered to determine from which compounds and at what operating conditions aerosol droplets are formed when the tobacco in the EHTP is heated. In particular, the role of compounds resulting from evaporation, such as *water*, *glycerol* and *nicotine*, on the aerosol formation were studied to evaluate if aerosol droplet nuclei can be formed with and without the effect of these major aerosol constituents, i.e. if aerosol droplet nuclei can form from chemical compounds potentially derived from the thermal degradation of tobacco components.

The paper is organized as follows. First, an overview of the aerosol dynamics modeling approach is given in Section II. Thereafter, analyzes of the operating conditions in the EHTS and in the EHTP are carried out in Section III followed by descriptions of the simulation cases in Section IV. The results from the simulations are presented and discussed in Section V. Finally, the outcome of the work is concluded in Section VI.

II. Modeling of Aerosol Dynamics

In this section, the general framework developed for multicomponent aerosol formation and evolution, applicable to large numbers of species at low computational effort is presented. This is an extension of the computational framework developed by [6], [7] for single component aerosol dynamics and presented by [14] for multicomponent aerosols. An aerosol is composed of droplets dispersed in a gas mixture [2]. This multicomponent gas-liquid phase mixture is further referred to as a fluid, irrespectively of its composition or the amount of gas or liquid phase components. In this work, both the gas and the liquid (droplet) phases of the fluid are treated as continua and modeled in an Eulerian-Eulerian framework. Moreover, the droplets are assumed to be sufficiently small, to precisely follow the flow, i.e., the relative velocity with respect to the carrier phase can be neglected. Likewise, the droplets are assumed to have immediate heat transfer with the carrier phase such that the temperature of all phases may be treated as being the same. Effects of phase changes are represented by the enthalpy of vaporization. With these underlying assumptions, the general system of governing equations describing the formation and evolution of a multicomponent aerosol can be expressed as [14]:

$$\begin{aligned}
\partial_t\rho + \partial_j(\rho u_j) &= 0 \\
\partial_t(\rho u_i) + \partial_j(\rho u_i u_j) &= -\partial_i p + \partial_j \tau_{ij} \quad ; \quad i = 1, ..., 3 \\
\rho c_p\Big(\partial_t T + u_j \partial_j T\Big) &= -\partial_j q_j - \tau_{kj}\partial_k u_j + S_h + \frac{Dp}{Dt} \\
\partial_t(\rho Y_i) + \partial_j(\rho Y_i u_j) &= -\partial_j j_{j,i} + S_i^{l\to v} \quad ; \quad i = 1, ..., n \\
\partial_t(\rho Z_i) + \partial_j(\rho Z_i u_j) &= -S_i^{l\to v} \quad ; \quad i = 1, ..., n \\
\partial_t(N) + \partial_j(N u_j) &= S_N
\end{aligned} \tag{1}$$

where ∂_t and ∂_j denote partial differentiation with respect to time t and spatial coordinate x_j respectively, and summation over j and k is implied, while no summation over i is adopted. The total mass density of the n-component system is denoted by ρ, velocity component by u_i and temperature by T. The material derivative of the pressure Dp/Dt contributes directly to changes in the local temperature. The heat capacity at constant pressure is denoted by c_p. The rate of strain tensor is given by

$$\tau_{ij} = \mu(\partial_j u_i + \partial_i u_j) - (\frac{2}{3}\mu - \kappa)\delta_{ij}\partial_k u_k \tag{2}$$

where μ is the dynamic viscosity of the mixture, δ_{ij} is the Kronecker delta tensor, and κ is the dilatational viscosity. The heat flux $q_j = -\lambda\partial_j T + \sum_{i=1}^{n} \bar{H}_i M_i^{-1} j_{j,i} + q_j^{(x)}$, where λ is the thermal conductivity of the mixture. $\bar{H}_i$ is the partial molar enthalpy of constituent i and $q^{(x)}$ is the usually negligible diffusion-thermo effect [15]. The molecular weight is denoted by M_i, the diffusion mass flux of constituent i is $j_{j,i} = \rho Y_i (u_{j,i} - u_j)$, where $u_{j,i}$ and Y_i are the diffusion velocity and mass fraction of component i in the gas phase, respectively. The mass fractions for the liquid phase of compound i is denoted Z_i. Soret and Dufour effects [15] were discarded in the present study. It is moreover assumed that the aerosol can be considered to be an ideal gas mixture, therefore connecting ρ, T, and p through the equation-of-state. The equation for the droplet number density N gives further information concerning the characterization of the aerosol. To preserve global mass in the system, the mass fraction equations sum up to the global mass conservation equation, leading to the following mass fraction and diffusion fluxes constraints:

$$\sum_{i=1}^{n}(Y_i + Z_i) = 1 \tag{3}$$

$$\sum_{i=1}^{n}\partial_j j_{j,i} = 0 \tag{4}$$

respectively. Note that droplet diffusion is neglected here. The aerosol in this work is modeled assuming a fixed log-normal aerosol size distribution, as is commonly done in moment equation models [2]. Transport of liquid mass fractions together with the evolving droplet number density provide information about the average aerosol droplet size. This may vary depending on the mass transfer (condensation/evaporation) and transport (convection and coalescence) processes in the system. Nucleation of aerosol affects both mass and droplet number density.

The source term related to the mass transfer between the liquid and the gas phase of species i is denoted by $S_i^{l\to v}$. This term contains two contributions: the nucleation mass flow rate S_i^{nuc}, characterizing gas changing into liquid, and the mass flow rate due to evaporation from already formed droplets minus that due to condensation onto these droplets, S_i^{e-c}, such that

$$S_i^{l\to v} = -S_i^{\text{nuc}} + S_i^{e-c} \tag{5}$$

The source term related to the heat flow rate due to phase change is denoted by S_h and can be computed by summing the products of $S_i^{l\to v}$ of species i with the heat of vaporization

of that species Δh_i^{vap} according to:

$$S_h = -\sum_{i=1}^{n} \Delta h_i^{\text{vap}} S_i^{l \to v} \tag{6}$$

Lastly the rate of change of the number concentration of droplets can be expressed as:

$$S_N = J_N - J_c - J_{ev} \tag{7}$$

in which the nucleation rate J_N, the coalescence rate J_c, and the rate of complete droplet evaporation J_{ev} can be distinguished. In this work, the effects of evaporation, condensation and coalescence are neglected, because the main focus is to determine if nucleation occurs. The neglected physical mechanisms have an influence on the aerosol droplet size and droplet number density, but not directly on the initiation of the nucleation process [8], [1].

The nucleation mass flow rate, S_i^{nuc}, can be expressed as:

$$S_i^{\text{nuc}} = 2 J_N N_i M_i \tag{8}$$

where N_i is the number of molecules of component i in a critical (equilibrium) cluster. The nucleation rate J_N can be written as:

$$J_N = R_{av} Z c_{eq} \tag{9}$$

where Z is the Zeldovich factor, which characterizes the contribution of Brownian motion to the formation of a critical cluster [16]. Here, the approximation of Z proposed by [8] is adopted. The equilibrium concentration c_{eq} can be expressed as:

$$c_{eq} = \exp\Big(-\frac{\Delta G}{kT}\Big) \prod_{i=1}^{n} \Big(\frac{p_i^{\text{sat}}(T)}{kT} \exp\Big(\frac{s_i^{\text{mon}} \sigma_i}{kT}\Big)\Big)^{w_i} \tag{10}$$

by adopting a so-called 'self-consistent' normalization [17], which is mathematically consistent in the limits of single species conditions [18]. Boltzmann's constant is denoted by k, the saturation vapor pressure of compound i by p_i^{sat} , and s_i^{mon} is the single compound, or 'monomer' surface area calculated from the partial molar volume of component i. The Gibbs free energy barrier of the critical cluster is denoted by ΔG, and w_i and σ_i are the mole fraction and surface tension of component i, respectively. By extending the ternary expression proposed by [8] to a general system of n components, the average growth rate R_{av} can be written as:

$$R_{av} = \frac{\sum_{i=1}^{n} N_i^2}{\sum_{i=1}^{n} N_i^2 / K_{ii}} \tag{11}$$

Moreover, under the assumption that cluster–cluster collisions can be neglected, i.e., in the sufficiently dilute state, the expression for the condensation rate K_{ii} proposed by [8] can be applied.

The governing equations and the related submodels are implemented into the extended PISO algorithm for aerosol dynamics developed by [6], [7] using the OpenFOAM® open source software package version 2.3.0. The algorithm is a segregated, collocated variable FV-based algorithm based on the original PISO algorithm [19].

III. Analyzes of Operating Conditions in the EHTS

In order to replicate the aerosol formation and dynamics inside the EHTP during use, the thermodynamic and operating conditions need to be estimated and represented. For example, it is important to accurately represent:

1) the flow, pressure and temperature conditions to achieve representative environmental conditions and cooling rates,
2) the thermophysical and chemical properties of representative compounds of the aerosol mixture to represent the physical characteristics of the individual constituents in the system at relevant temperatures,
3) the composition of the multicomponent aerosol mixture to account for a realistic aerosol in the simulations.

In the following subsections, estimations of these conditions and parameters are carried out for the EHTP for relevant operating conditions.

A. Flow Condition

The flow condition in the EHTP can be estimated by computing a representative velocity from the aerosol generation profile applied during the use of the product. The flow path through the EHTP when air is drawn through it is shown in Fig. 1. A typical aerosol generation protocol starts by inhaling a volume V_{puff} during a time Δt_{puff}. The puff is then followed by a pause before the next puff is taken Δt_{ip} after the previous puff start. This is repeated for N_{puff} to complete the protocol. From this general aerosol generation protocol, an average volumetric flow rate Q_{avg} can be calculated from:

$$Q_{\text{avg}} = \frac{V_{\text{puff}}}{\Delta t_{\text{puff}}} \tag{12}$$

Based on the effective cross-sectional area A_{cs}^{eff}, through which the fluid flows, an average velocity U_{avg} can be calculated according to:

$$U_{\text{avg}} = \frac{Q_{\text{avg}}}{A_{cs}^{\text{eff}}} \tag{13}$$

As can be seen in (13), the velocity may take different values depending on A_{cs}^{eff}. A_{cs}^{eff} varies along the centerline of an EHTP. For example, the A_{cs}^{eff} can generally be expressed as:

$$A_{cs}^{\text{eff}} = \frac{\phi \pi d_{cs}^2}{4} \tag{14}$$

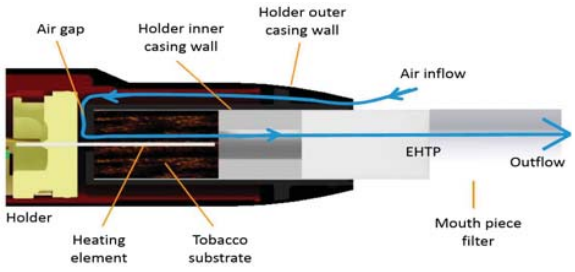

Fig. 1 Flow path in the EHTP during use in the Holder heating device

TABLE I
PARAMETERS OF THE HEALTH CANADA INTENSE REGIME N_{PUFFS} IS SET BY THE EHTS AND Q_{AVG} IS CALCULATED FROM (12)

V_{puff}/ (mL)	Δt_{puff}/ (s)	N_{puffs}	Δt_{ip}/ (s)	$Q_{\text{avg}}^{(\text{HCI})}$/ (mL s^{-1})
55.0	2.0	12	30	**27.5**

TABLE II
REPRESENTATIVE PARAMETERS OF THE EHTP. $U_{\text{AVG}}^{(\text{TP})}$ AND $U_{\text{AVG}}^{(\text{ET})}$ ARE CALCULATED FROM (13) USING THEIR RESPECTIVE INPUT PARAMETERS

Tobacco plug (TP)		Empty tube (ET)	
$\phi^{(\text{TP})}$	0.3	$\phi^{(\text{ET})}$	1.0
$d_{cs}^{(\text{TP})}$/(mm)	7.2	$d_{cs}^{(\text{ET})}$/(mm)	7.2
$f^{(\text{TP})}$	~ 0.5	$f^{(\text{ET})}$	1.0
L/ (mm)	~ 10	L/ (mm)	~ 10
$U_{\text{avg}}^{(\text{TP})}$/ (m s^{-1})	$\sim$**9.0**	$U_{\text{avg}}^{(\text{ET})}$/ (m s^{-1})	$\sim$**0.7**

where ϕ is the porosity of the porous tobacco plug or filter and d_{cs} is the diameter of the cross-section through which the fluid effectively flows through. In porous parts of the EHTP, $\phi \in (0, 1)$ and in pure fluid regions, $\phi = 1$.

Estimation of Representative Velocities: Because the flow in the EHTP is spatially nonuniform, typical flow conditions need to be determined. For this, a Health Canada Intense (HCI) aerosol generation protocol [20] is adopted. The values of the parameters V_{puff}, Δt_{puff}, $N_{\text{puff}s}$, and Δt_{ip} for this protocol are tabulated in Table I. Inserting the values from Table I into (12) results in a volumetric flow rate for the HCI regime being $Q_{\text{avg}}^{(\text{HCI})}$.

Two conditions for the estimation of representative velocities in the EHTP are considered, namely (i) the *flow in the tobacco plug* and (ii) in an *empty tube* with the diameter of the EHTP, see Fig. 1. The latter case is considered, because aerosol may form outside of the tobacco plug when the warm multicomponent gas mixture is mixed with cooler air.

(i) *Tobacco plug (TP):* The average intrinsic velocity in the tobacco plug $U_{\text{avg}}^{(\text{TP})}$ can be computed from (13) using Q_{avg} from Table I and A_{cs}^{eff} from (14) with $\phi = \phi^{(\text{TP})}$, $d_{cs} = f^{(\text{TP})} d_{cs}^{(\text{TP})}$, where d_{cs} is the EHTP diameter and f is the fraction of the diameter, where the fluid flows due to the inlet restriction in the EHTS design, cf. Fig. 1. Estimated representative values of these parameters can be found in Table II. The representative intrinsic velocity in the tobacco plug can therefore be calculated to be $U_{\text{avg}}^{(\text{TP})}$, cf. Table II.

(ii) *Empty tube (ET):* The average intrinsic velocity in an empty tube $U_{\text{avg}}^{(\text{ET})}$ of diameter $d_{cs} = f^{(\text{ET})} d_{cs}^{(\text{ET})}$ can be calculated using (13) and (14) with the values $Q_{\text{avg}}^{(\text{HCI})}$, $\phi = \phi^{(\text{ET})}$, $f^{(\text{ET})}$, and $d_{cs}^{(\text{ET})}$ from Table I and II.

With the representative velocities estimated, the next step before determining the representative cooling rates in the system is to analyze the temperature conditions in the system.

TABLE III
REPRESENTATIVE OPERATING CONDITIONS FOR THE HOLDER HEATING DEVICE. A PRESSURE DROP OF $50mmH_2O$ IS ACCOUNTED FOR IN THE TABULATED OPERATING PRESSURE VALUE p_0

Parameters	
T_{amb} / (K)	303.15 (30°C)
T_h / (K)	623.15 (350°C)
p_0 / (Pa)	100835

B. Temperature Condition

The temperature in the EHTP ranges from ambient temperature T_{amb} up to the heater set temperature T_h of the Holder (heating device) [21], see Table III. The temperature is both temporally and spatially varying between the highest and the lowest value, with the highest value being close to the heating element and the lowest temperature at the perimeter and at the outlet of the EHTP or of the incoming ambient air. The temperature non-uniformity in the system implies that strong temperature gradients and cooling rates are present in the EHTP during use, when the fluid is flowing through the product. It is this cooling of the multicomponent gas mixture that initiates the nucleation process leading to the formation of aerosol droplets. Combining the estimates of the representative velocities in the system and the extremities of the temperature range, the cooling rate that the gas mixture experiences in the system can be estimated.

Estimation of Cooling Rates: Representative cooling rates in the EHTP when heated in the Holder can be calculated using the estimated velocities and temperatures presented in Tables II and III. The cooling rate $\frac{dT}{dt}$ can be estimated from:

$$\frac{dT}{dt} \approx -(T_h - T_{\text{amb}}) \frac{U_{\text{avg}}}{L} \tag{15}$$

where L is the length at which the temperature is decreased from T_h to T_{amb}. As mentioned previously, the highest temperature T_h is the temperature of the heating element. The ambient temperature, representing the lowest temperature in the system, is in this work estimated to the tabulated value in Table III, which represents a typical aerosol temperature exiting the EHTP. In terms of the representative length scale L for the cooling process, it is estimated to be of the order of the distance between the end of the tobacco plug and the mouth piece filter (approximately $10mm$). This estimated length is used for both the *tobacco plug* and the *empty tube* scenarios. This length may be slightly smaller considering mixing of the incoming cooler air with the warmer air flowing in the vicinity of the heating element. This estimate has more influence on the final droplet number density than the actual nucleation process itself and has therefore minor influence on the simulation results related to the formation of aerosol droplet nuclei.

Applying the estimated average intrinsic velocities and the length scales presented in Table II, the two extremities of the cooling rates $\left(\frac{dT}{dt}\right)_{\text{low}}$ and $\left(\frac{dT}{dt}\right)_{\text{high}}$ takes the values reported in Table IV. The subscripts low and $high$ refers to the magnitude of the cooling rates.

TABLE IV
ESTIMATED HIGH AND LOW COOLING RATE IN THE EHTP WHEN HEATED (IN THE HOLDER)

Cooling rates	
$\left(\frac{dT}{dt}\right)_{\text{low}}$ / (K s^{-1})	$\sim -2.2 \cdot 10^4$
$\left(\frac{dT}{dt}\right)_{\text{high}}$ / (K s^{-1})	$\sim -2.9 \cdot 10^5$

C. Compounds Represented in the Multicomponent Aerosol

The multicomponent aerosol resulting from the use of an EHTP has been shown to be significantly less complex (fewer compounds and reduced concentrations) compared to smoke generated from burning tobacco [22], [21]. Labstat International ULC, 262 Manitou Dr., Kitchener, ON N2C 1L3, Canada, an independent ISO 17025 accredited contract research organization, performed analytical experiments to assess any contribution of combustion to processes occurring in the EHTP. During these experiments, the product was heated under atmospheres of nitrogen and synthetic air and a selection of 35 compounds were quantified from collections of the EHTP aerosol generated using a HCI aerosol generation protocol. The total mass of each compound determined by Labstat International ULC under an atmosphere of synthetic (dry) air, cf. Table V, are used in the following simulation scenarios A through E so that the presence of water in the incoming air can be excluded from playing a role in the aerosol nucleation process. To model the aerosol generation and evolution from a gas mixture of the 35 compounds, the thermophysical properties need to be determined for each constituent. Moreover, since the aerosol generation and evolution process takes place in strongly varying temperature conditions as discussed previously, the temperature dependence of the thermophysical properties need also to be accounted for whenever possible. Among the 35 measured and reported compounds by Labstat International ULC, temperature dependent thermophysical properties for the compounds tabulated in Table V were collected from the databases [23], [24]. For the compounds: *benzo[a]pyrene*, *hydroquinone*, *1-aminonaphthalene*, *2-aminonaphthalene*, *3-aminobiphenyl*, and *4-aminobiphenyl*, no data of their thermophysical properties were found. These compounds are therefore not considered in this work. The data of the thermophysical properties extracted from [23] are given as coefficients to VDI equations [23] for the various compounds and properties. The data taken from the Cameochemicals database are fitted to National Standard Reference Data Series (NSRDS) functions [25] for the various properties. As an example, the temperature dependent saturation pressure curves are shown for all considered compounds in Fig. 2.

The major characterized compounds in terms of their masses were *water*, *glycerol* and *nicotine*, as shown in Table V. These constituents originate from the tobacco plug in the EHTP and when the tobacco substrate is heated, these constituents are released and evaporated intact to the gas phase. *Glycerol* has been added to the tobacco substrate, as an aerosol former,

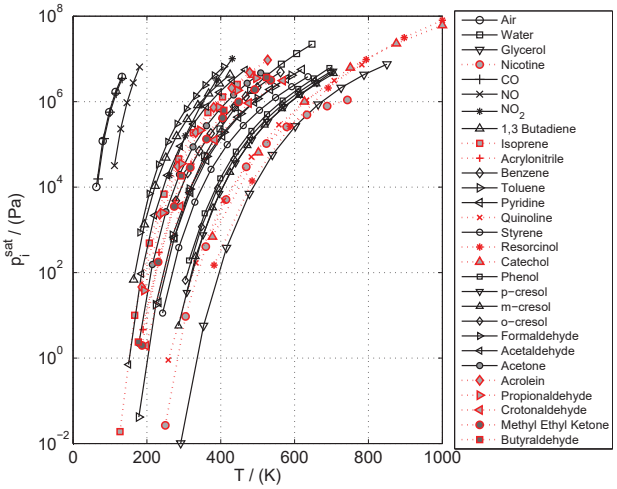

Fig. 2 Saturation vapor pressures of compounds. The data plotted with black continuous lines are taken from [23] and the those plotted with red dotted lines are taken from [24]

to aid the formation of an aerosol at the lower operating temperature range of the tobacco in the EHTP compared to cigarettes. In addition to the quantified compounds reported in Table V, the total particulate matter (TPM) was collected by Labstat International ULC and quantified to be $55.2mg$ for the entire HCI puffing regime. Subtracting the quantified masses of the compounds in Table V, except for the masses of the highly volatile gas-phase compounds *carbon monoxide*, *nitric oxide* and *nitrogen dioxide*, the total remaining mass can be determined to be $m_{uc} = 11.8mg$ per unit. This mass is excluded from the simulations in *case A* and *case B*, because the type and the thermophysical properties of the compounds present in this weight fraction are unknown. This omitted mass is however taken into account in the *case C*, as explained in detail below, to ensure that the total mass of TPM is accounted for in the simulation and is even largely surpassed in *case D* and *case E*.

Based on the thermophysical properties for the individual constituents of the multicomponent mixture, the bulk thermophysical properties of the aerosol are determined using mixture laws for multicomponent mixtures in accordance with [15], [26].

To determine the composition of the gas mixture prior to the nucleation process, the mass of the carrier gas, i.e. the synthetic air, flowing though the product during use needs to be accounted for. The mass of air flowing through the product during use can be calculated from the density of the air at ambient conditions and the volumetric flow rate and puff duration according to:

$$m_{\text{air}} = Q_{\text{avg}} \Delta t_{\text{puff}}(\rho_{\text{air}})|_{T=303.15K} \tag{16}$$

Furthermore, to compute the initial mass fractions of the multicomponent gas mixture, there are five scenarios considered in this work:

A The experimentally measured masses of the compounds listed in Table V are assumed to be evenly distributed

over all N_{puffs} puffs with all compounds listed in Table V in the initial multicomponent gas mixture. All compounds except for *air* are considered to be phase-changing and may contribute to the nucleation process forming aerosol droplets.

B The same composition as in the *case A* above is assumed, but the compounds originating from the tobacco by evaporation, such as *water*, *glycerol* and *nicotine*, are considered to be present in the aerosol but inert and can therefore not contribute to the aerosol droplet formation. The intent of this case is to investigate if the other compounds in the gas mixture (generated from thermal decomposition of tobacco components) can form aerosol droplets on their own, without the help of aerosol formers released from the tobacco by evaporation.

C This case is identical to the *case B* above, but the masses of the minor compounds are increased by a factor of 50, as seen in Table V. This 50-fold increase of the amounts of the minor compounds represents a total mass of $18.2mg$ of these compounds, which is approximately 1.5 times the total mass remainder ($m_{uc} = 11.8mg$) reported by Labstat International ULC and omitted in the simulation *cases A* and *B*. This implies that all m_{uc} is accounted for and approximated by the masses of the minor compounds in Table V.

D This case is identical to the *case B* above, but the masses of the minor compounds are increased by a factor of 100, as seen in Table V. This case represents a situation where the amount of the minor compounds are largely increased to a total mass of $36.4mg$, representing a situation where all the mass of the minor components appears during roughly $1/8$ of the duration of a single puff of $2s$. Furthermore, the collected mass of the minor compounds in this case is almost equal to the mass of *water*, cf. Table V.

E This case is identical to the *case B* above, but the masses of the minor compounds are increased by a factor of 500, as seen in Table V. This 500-fold increase of the minor compounds represents a total mass of $182mg$ of these compounds distributed over the HCI protocol. The goal of this extreme case is to investigate the sensitivity of the nucleation process and to estimate the likelihood of aerosol droplets being generated from the minor components of the gas mixture presented in Table V under the operating conditions of the Holder (heating device) and without the help of an aerosol former.

The idea of the *cases C-E* is to see if significantly increasing the mass fraction of minor compounds present in the gas phase leads to the formation of aerosol droplets on their own without the help of aerosol formers derived from the tobacco substrate by evaporation processes.

The mass fractions of the various compounds, assuming an initially pure multicomponent gas mixture, can be computed from:

$$Y_i^{\text{init}} = \frac{m_i}{\sum_{i=1}^{n} m_i} \tag{17}$$

TABLE V
CONSIDERED COMPOUNDS AND THEIR MASSES PRESENT IN THE EHTP AEROSOL ACCUMULATED DURING 12 PUFFS. THE MASS OF AIR IS CALCULATED BASED ON THE HCI REGIME. THE COMPOUNDS MARKED BY A * INDICATES THAT THEY ARE INERT AND CANNOT CONTRIBUTE TO THE FORMATION OF AEROSOLS FOR ANY OF THE CASES, WHEREAS THE COMPOUNDS MARKED BY ** ARE TREATED AS INERT IN THE CASES B-E, WHEREAS THEY ARE PHASE CHANGING IN CASE A. THE MASSES FOR THE CASES C-E INDICATE HOW MANY TIMES MORE THE MASSES ARE COMPARED TO IN THE CASES A AND B

Compound	Cases A, B	Case C	Case D	Case E
	$m/(\mu g)$	$m/(\mu g)$	$m/(\mu g)$	$m/(\mu g)$
Air*	$7.95 \cdot 10^5$	$\times 1$	$\times 1$	$\times 1$
Water**	$3.73 \cdot 10^4$	$\times 1$	$\times 1$	$\times 1$
Glycerol**	$4.39 \cdot 10^3$	$\times 1$	$\times 1$	$\times 1$
Nicotine**	$1.37 \cdot 10^3$	$\times 1$	$\times 1$	$\times 1$
Carbon monoxide	$0.54 \cdot 10^3$	$\times 50$	$\times 100$	$\times 500$
Nitric oxide	19.9	$\times 50$	$\times 100$	$\times 500$
Nitrogen dioxide	0.9	$\times 50$	$\times 100$	$\times 500$
1,3-Butadiene	0.3	$\times 50$	$\times 100$	$\times 500$
Isoprene	2.3	$\times 50$	$\times 100$	$\times 500$
Acrylonitrile	0.2	$\times 50$	$\times 100$	$\times 500$
Benzene	0.6	$\times 50$	$\times 100$	$\times 500$
Toluene	2.0	$\times 50$	$\times 100$	$\times 500$
Pyridine	7.8	$\times 50$	$\times 100$	$\times 500$
Quinoline	0.011	$\times 50$	$\times 100$	$\times 500$
Styrene	0.7	$\times 50$	$\times 100$	$\times 500$
Resorcinol	0.055	$\times 50$	$\times 100$	$\times 500$
Catechol	14.3	$\times 50$	$\times 100$	$\times 500$
Phenol	1.4	$\times 50$	$\times 100$	$\times 500$
p-cresol	0.07	$\times 50$	$\times 100$	$\times 500$
m-cresol	0.03	$\times 50$	$\times 100$	$\times 500$
o-cresol	0.06	$\times 50$	$\times 100$	$\times 500$
Formaldehyde	9.1	$\times 50$	$\times 100$	$\times 500$
Acetaldehyde	230	$\times 50$	$\times 100$	$\times 500$
Acetone	35.9	$\times 50$	$\times 100$	$\times 500$
Acrolein	10.7	$\times 50$	$\times 100$	$\times 500$
Propionaldehyde	14.9	$\times 50$	$\times 100$	$\times 500$
Crotonaldehyde	3.29	$\times 50$	$\times 100$	$\times 500$
Methyl Ethyl Ketone	7.6	$\times 50$	$\times 100$	$\times 500$
Butyraldehyde	23.1	$\times 50$	$\times 100$	$\times 500$

using the tabulated masses in Table V. The resulting mass fractions for the five cases are reported in Table VI.

IV. CASE DESCRIPTIONS

A. Geometry

The geometry considered in this work is represented in one dimension, with the spatial $x-$coordinate direction as depicted in Fig. 3. This case is a one-dimensional representation of the geometry used in [7] and represents the flow path through the EHTP indicated in Fig. 1. The geometry spans from the inlet placed at $x = x_0$ to the outlet located at $x = x_3$. Three regions of the geometry are defined, where the regions $R1$, $R2$ and $R3$ range from $x \in [x_0, x_1)$, $x \in [x_1, x_2)$, and $x \in [x_2, x_3]$, respectively. This gives the lengths of the three regions $L_{R1} = x_1 - x_0$, $L_{R2} = x_2 - x_1$, and $L_{R3} = x_3 - x_2$, respectively. The region $R1$ is represented as

TABLE VI
GAS PHASE MASS FRACTIONS Y_i^{inert} OF THE COMPOUNDS IN THE EHTP AEROSOL CALCULATED FROM THE MASSES IN TABLE V USING (17) ASSUMING A PURE GAS MIXTURE. THESE MASS FRACTIONS ARE USED AS INITIAL CONDITIONS IN THE SIMULATIONS. THE COMPOUNDS MARKED BY A * INDICATES THAT THEY ARE INERT AND CANNOT CONTRIBUTE TO THE FORMATION OF AEROSOLS FOR ANY OF THE CASES, WHEREAS THE COMPOUNDS MARKED BY ** ARE TREATED AS INERT IN THE CASES B-E, WHEREAS THEY ARE PHASE CHANGING IN CASE A. THE MASS FRACTIONS FOR THE CASES C-E INDICATE HOW MANY TIMES MORE THE MASS FRACTIONS ARE COMPARED TO IN THE CASES A AND B

Compound	**Cases A, B**	**Case C**	**Case D**	**Case E**
	Y_i^{init}	Y_i^{init}	Y_i^{init}	Y_i^{init}
Air*	$9.4464 \cdot 10^{-1}$	0.88759	0.82937	0.36360
Water**	$4.6943 \cdot 10^{-2}$	$\times 1$	$\times 1$	$\times 1$
Glycerol**	$5.5250 \cdot 10^{-3}$	$\times 1$	$\times 1$	$\times 1$
Nicotine**	$1.7242 \cdot 10^{-3}$	$\times 1$	$\times 1$	$\times 1$
Carbon monoxide	$6.7961 \cdot 10^{-4}$	$\times 50$	$\times 100$	$\times 500$
Nitric oxide	$2.5045 \cdot 10^{-5}$	$\times 50$	$\times 100$	$\times 500$
Nitrogen dioxide	$1.1327 \cdot 10^{-6}$	$\times 50$	$\times 100$	$\times 500$
1,3-Butadiene	$3.7756 \cdot 10^{-7}$	$\times 50$	$\times 100$	$\times 500$
Isoprene	$2.8946 \cdot 10^{-6}$	$\times 50$	$\times 100$	$\times 500$
Acrylonitrile	$2.5171 \cdot 10^{-7}$	$\times 50$	$\times 100$	$\times 500$
Benzene	$7.5512 \cdot 10^{-7}$	$\times 50$	$\times 100$	$\times 500$
Toluene	$2.5171 \cdot 10^{-6}$	$\times 50$	$\times 100$	$\times 500$
Pyridine	$9.8166 \cdot 10^{-6}$	$\times 50$	$\times 100$	$\times 500$
Quinoline	$1.3844 \cdot 10^{-8}$	$\times 50$	$\times 100$	$\times 500$
Styrene	$8.8097 \cdot 10^{-7}$	$\times 50$	$\times 100$	$\times 500$
Resorcinol	$6.9219 \cdot 10^{-8}$	$\times 50$	$\times 100$	$\times 500$
Catechol	$1.7997 \cdot 10^{-5}$	$\times 50$	$\times 100$	$\times 500$
Phenol	$1.7619 \cdot 10^{-6}$	$\times 50$	$\times 100$	$\times 500$
p-cresol	$8.8097 \cdot 10^{-8}$	$\times 50$	$\times 100$	$\times 500$
m-cresol	$3.7756 \cdot 10^{-8}$	$\times 50$	$\times 100$	$\times 500$
o-cresol	$7.5512 \cdot 10^{-8}$	$\times 50$	$\times 100$	$\times 500$
Formaldehyde	$1.1453 \cdot 10^{-5}$	$\times 50$	$\times 100$	$\times 500$
Acetaldehyde	$2.8946 \cdot 10^{-4}$	$\times 50$	$\times 100$	$\times 500$
Acetone	$4.5181 \cdot 10^{-5}$	$\times 50$	$\times 100$	$\times 500$
Acrolein	$1.3466 \cdot 10^{-5}$	$\times 50$	$\times 100$	$\times 500$
Propionaldehyde	$1.8752 \cdot 10^{-5}$	$\times 50$	$\times 100$	$\times 500$
Crotonaldehyde	$4.1406 \cdot 10^{-6}$	$\times 50$	$\times 100$	$\times 500$
Methyl Ethyl Ketone	$9.5649 \cdot 10^{-6}$	$\times 50$	$\times 100$	$\times 500$
Butyraldehyde	$2.9072 \cdot 10^{-5}$	$\times 50$	$\times 100$	$\times 500$

an inlet region $R1$ of arbitrarily length, see Table VII, before the cooling region $R2$ representative of the cooling region in the EHTP, cf. Fig. 1. The last region, $R3$, is defined for the aerosol generation process to have time to reach a constant, quasi-steady condition. The lengths of the regions $R1$ and $R3$ are not intended to be representative to any specific lengths of the EHTP and are only specified for computational purposes. The values of the spatial positions x_i is tabulated in Table VII. The chosen values are based on the flow and temperature conditions described previously to reach representative cooling rates for the multicomponent gas mixture.

B. Computational Mesh

The one-dimensional geometry is discretized using hexahedral elements, because of the FV method used to solve the discretized governing equations. The geometrical representation in the y- and z-directions spans over $y \in [-y_1, y_1]$ and $z \in [-z_1, z_1]$, respectively. The number of hexahedral elements in the regions $R1$, $R2$ and $R3$ are denoted N_{R1}, N_{R2}, and N_{R3}, respectively. Their respective values can be found in Table VII.

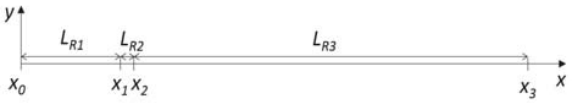

Fig. 3 Geometry

TABLE VII
GEOMETRIC AND SIMULATION PARAMETERS

Geometric		*Simulation*	
$x_0/(m)$	0.00	N_{R1}	100
$x_1/(m)$	0.10	N_{R2}	10
$x_2/(m)$	0.11	N_{R3}	400
$x_3/(m)$	0.51	Co	0.2
$y_1 = z_1/(m)$	10^{-4}	$\Delta t_{ts}^{\max}/(s)$	10^{-5}
$L_{R1}/(m)$	0.10	$t_s/(s)$	0.0
$L_{R2}/(m)$	0.01	$t_e/(s)$	0.01
$L_{R3}/(m)$	0.40	$t_{\text{end}}/(s)$	1.5

C. Simulation Conditions

In order to simulate the nucleation process, a multicomponent gas mixture with gas-phase mass fractions according to Table VI was initially set at an elevated temperature T_h cf. Table III. This uniform initial state is important, because a pressure-based compressible algorithm is used and consistent initial conditions are crucial. The temperature is artificially specified on the walls with normal vectors directed perpendicular to the x-direction. The wall temperature is then gradually reduced in the regions $R2$ and $R3$ using the function:

$$T(x,t) = \begin{cases} T_h, & \text{if } x_0 \le x < x_1 \\ T^\star(t) + \frac{T^\star(t) - T_{\text{amb}}}{x_2 - x_1}, & \text{if } x_1 \le x < x_2 \\ T^\star(t), & \text{if } x_2 \le x \le x_3 \end{cases} \quad (18)$$

where

$$T^\star(t) = \begin{cases} T_h, & \text{if } t < t_s \\ T_h + \frac{T_h - T_{\text{amb}}}{t_s - t_e}, & \text{if } t_s \le t < t_e \\ T_{\text{amb}}. & \text{if } t_e \le t \le t_{\text{end}} \end{cases} \quad (19)$$

The temperature boundary conditions at the inlet (at x_0) and at the outlet (at x_3) are specified as zero gradient in the x-direction.

The x-component of the velocity is specified at x_0 and a zero gradient condition is applied at the outlet position x_3. A zero gradient pressure boundary condition is specified at the inlet, whereas a total pressure boundary condition is applied at the outlet with the total pressure value p_0 presented in Table III specified.

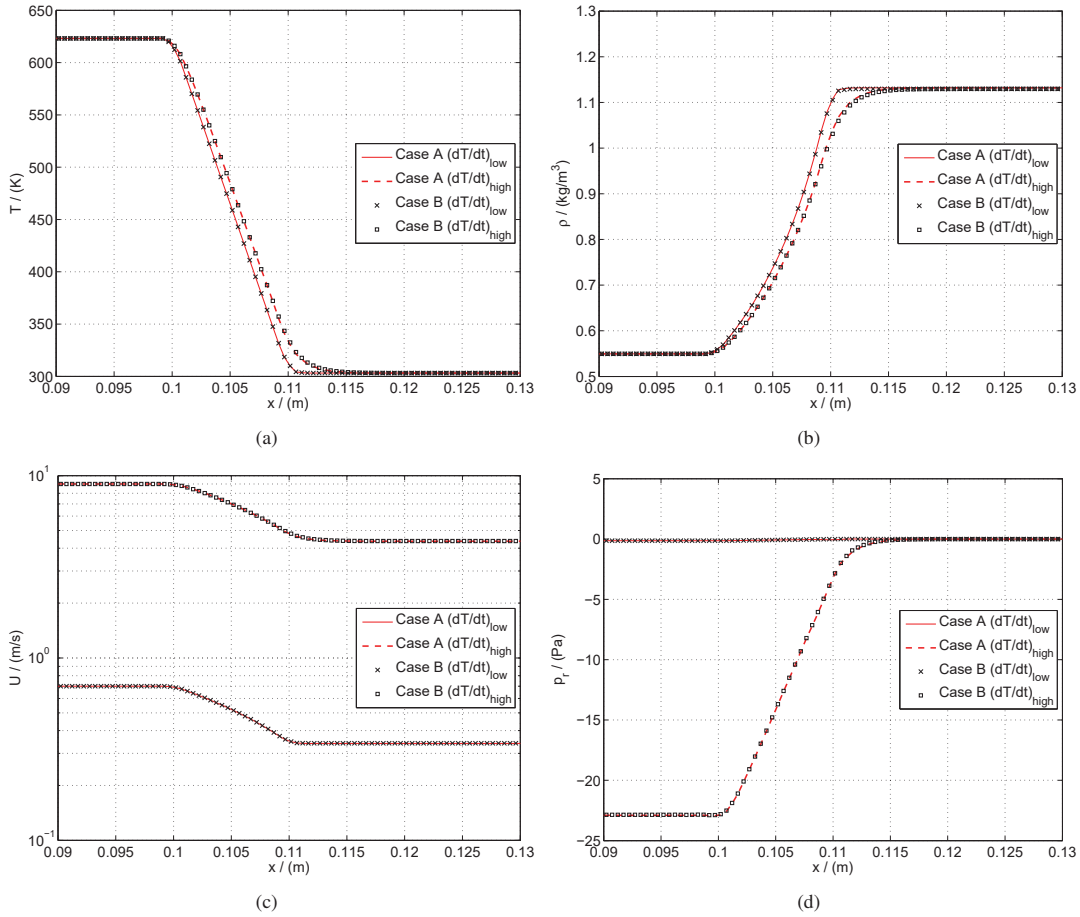

Fig. 4 a) Mixture temperature, b) aerosol density, c) velocity in the positive x-direction, and d) dynamic (relative) pressure for the cases A and B along the x-axis (around the cooling region) at the time t_{end}

The mass fractions of the gas phase for the various compounds are specified at the inlet based on the values specified in Table VI and a zero gradient condition is specified at the outlet. All liquid phase mass fractions are specified as zero at the inlet. Moreover, the droplet number density N is initiated as a zero field representing an initially pure multicomponent gas mixture without aerosol droplets. A zero droplet number density is specified at the inlet and a zero gradient condition is applied at the outlet. The conditions at the cell faces with normal vectors perpendicular to the x-direction are treated with a zero gradient condition to mimic a one-dimensional setting for all variables, except for the temperature as explained previously.

The physical end time of the simulation t_{end} presented in Table VII ensures that the aerosol dynamics reaches a quasi-steady state. The timestep of the time discretization is adaptive to ensure that the Courant (Co) number is kept below the value specified in Table VII. To ensure that physical processes limited by a small physical timestep are resolved also for cases with low velocity, a maximum allowed timestep Δt_{max} is set to the value specified in Table VII.

The time derivatives of the governing equations (1) are discretized by first-order accurate implicit Euler schemes and the convective terms by the second-order linear upwind differencing (LUD) scheme [27]. The Laplacian terms are discretized using linear schemes for the interpolation of the cell-centered field values to the face centers of the control volumes. The discretized momentum equations for each coordinate direction are solved using a Preconditioned Bi-Conjugate Gradient (PBiCG) linear solver with a Diagonal Incomplete Lower Upper (DILU) preconditioner down to the tolerance 10^{-12} and the pressure equation is solved with a Preconditioned Conjugate Gradient (PCG) solver with Diagonal Incomplete-Cholesky (DIC) preconditioner down to the tolerance 10^{-12}. The mass fraction equations, the transport equation for the droplet number density and the temperature equations are solved using the PBiCG solver with a DILU preconditioner. The temperature equation is solved down to a tolerance of 10^{-12}, whereas the mass fraction equations and the droplet number density transport equation are solved down to a tolerance of 10^{-14} to ensure converged results and mass conservation of all compounds.

V. Results & Discussion

It can be observed in Fig. 4 that the temperature, density, velocity and relative pressure are strongly coupled during the

aerosol generation and transport for the two cases A and B and for both the low and high cooling rates simulated. The imposed temperature change in the system via the boundary conditions results in a drop in temperature of the gas mixture along the positive x-axis, see Fig. 4a. This drop is slightly delayed for $\left(\frac{dT}{dt}\right)_{\text{high}}$, due to the higher velocity and its resulting higher convective energy flux. It can also be seen that the temperature changes similarly for the two cases A and B. The large temperature change in the system results in a strong increase of the aerosol mixture density, see Fig. 4b, due to thermal contraction as well as aerosol formation. In Fig. 4c, the velocities for the two cases A and B are shown along the x-axis for both the low and the high cooling rates. The velocities are reduced along the flow direction as a consequence of the change in density to ensure that mass is conserved in the system. The non-uniform density and velocity profiles are also reflected in the relative (dynamic) pressure p_r, see Fig. 4d, which highlights the strong coupling between the involved variables. Moreover, the influence of the cooling rate are shown to be small for all state variables presented in Fig. 4.

As mentioned previously in the case description, all compounds present in case A can contribute to the aerosol formation, except for *air*. Because the initial droplet number density is set to be zero for all compounds, a nonzero droplet number density indicates that aerosol droplet nuclei are formed from the supersaturated multicomponent gas mixture during the cooling phase. It can clearly be seen in Fig. 5 that according to CNT aerosol droplet nuclei are formed from the gas mixture in case A, whereas no aerosol droplet nuclei are formed from the gas mixture in case B, where *glycerol*, *nicotine*, and *water* are treated as inert and therefore not contributing to the nucleation process. The droplet number density along the x-axis shows that the nucleation process happens rapidly in the case A when the gas mixture is cooled down and the aerosol forming compounds are reaching their supersaturated states. The onset of the nucleation process is shown to occur at slightly different x-positions for the different cooling rates and is shown to result in only slightly different droplet number densities. This is a result of the large difference in velocities between the two cases and its resulting effect on the thermophysical states of the cases, as shown in Fig. 4. The fact that aerosol droplet nuclei are formed in case A but not in case B indicates that it is the effect of the aerosol formers (*glycerol*, *nicotine*, and *water*), being treated as inert in case B, that triggers the aerosol formation in case A. Therefore, excluding the effect of these aerosol formers implies that no aerosol droplet nuclei are formed from the minor compounds alone and that all of these compounds, potentially derived from thermal decomposition reactions, remain in their gas phases according to the extended CNT for multicomponent aerosols. As shown in Fig. 5, there is no significant influence of the cooling rate on the nucleation process. Therefore, only the low cooling rate is analyzed hereafter.

To determine which compounds are the major constituents in the generated aerosol droplets after the nucleation process, the liquid phase mass fractions can be studied for the various compounds presented in Table VI. It can be seen in Fig. 6, that among the phase-changing chemical species of group 1 of

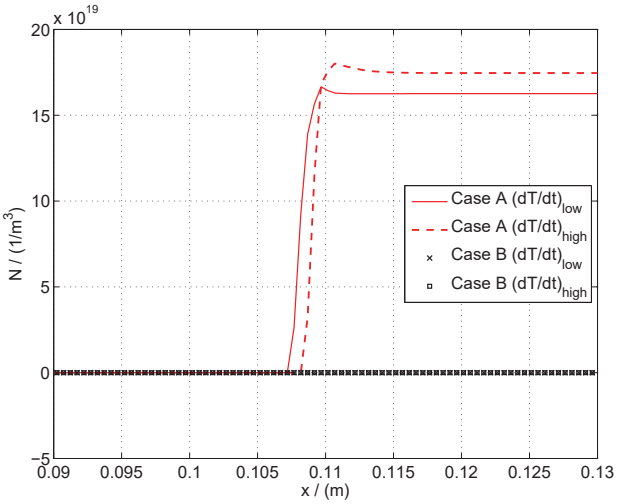

Fig. 5 Droplet number density for the cases A and B along the x-axis (around the cooling region) at t_{end}

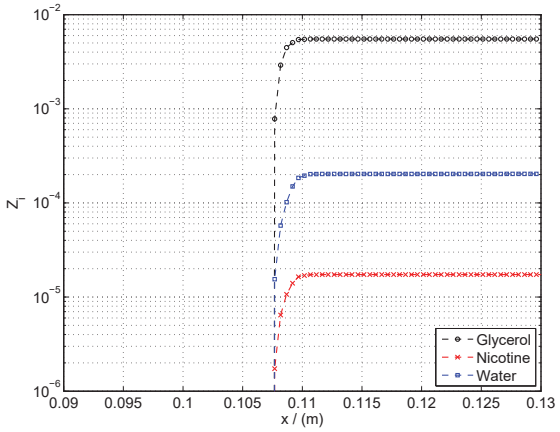

Fig. 6 Liquid phase mass fractions along the x-axis (around the cooling region) at t_{end} for case A with $\left(\frac{dT}{dt}\right)_{\text{low}}$ for the phase-changing compounds in group 1 of Table VI

Table VI, *glycerol* is the main phase-changing compound due to its highest liquid phase mass fraction Z_i. This high liquid mass fraction resulting from the nucleation process indicates that the generated critical clusters are mostly composed of liquid *glycerol*. The second most abundant compound in the generated aerosol droplet nuclei is *water*, followed by *nicotine*. Note that these reported values are the mass fractions of the aerosol droplet nuclei generated from the nucleation process and not the final composition after aerosol droplet evolution from condensation, evaporation and coalescence processes have been taken into account, which as mentioned previously have strong influence on the final composition of the aerosol droplets. Moreover, it can be seen that according to the extended CNT, the other (minor) compounds of Table VI have liquid mass fractions several orders of magnitudes lower than the three compounds discussed above, cf. Fig. 7. The fact that most compounds are present at a small amount in the aerosol

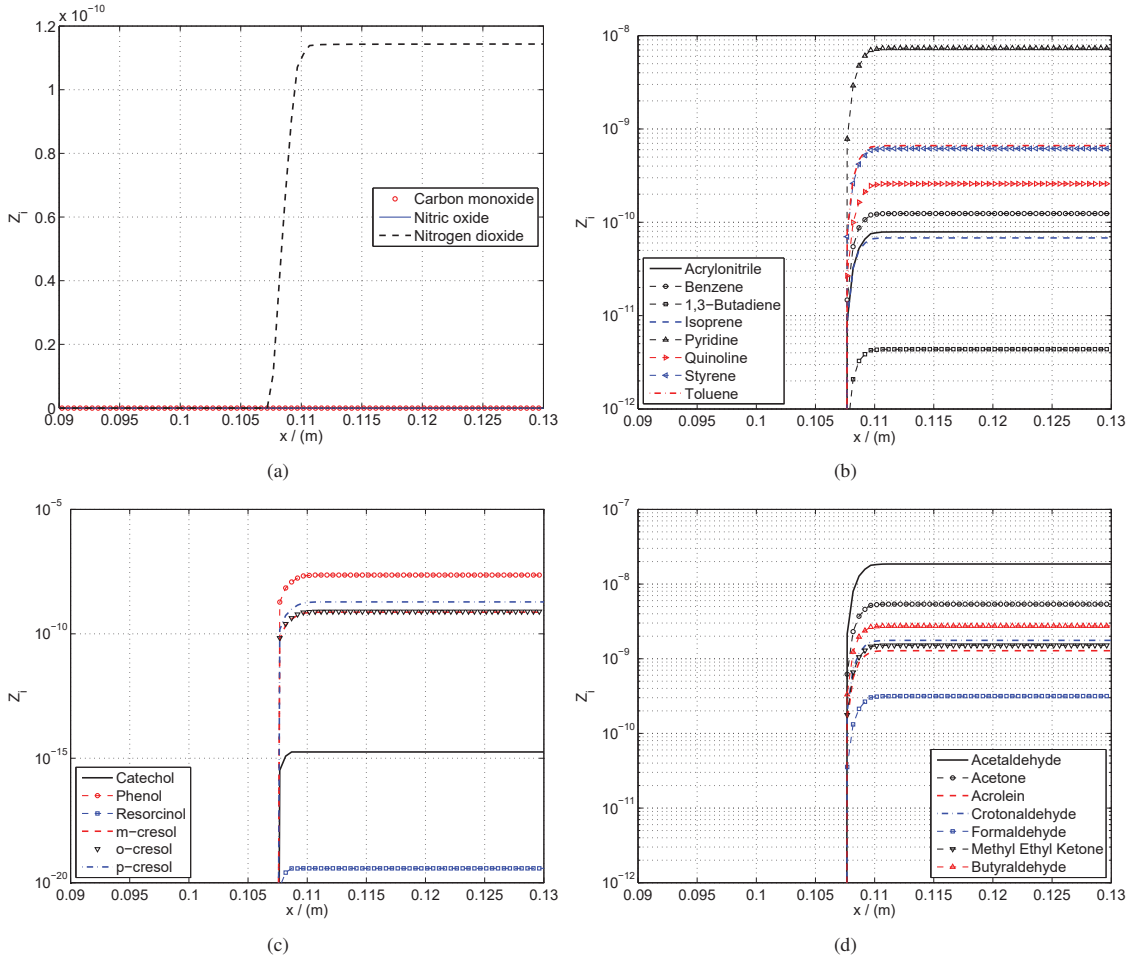

Fig. 7 Liquid phase mass fractions along the x-axis (around the cooling region) at t_{end} for case A with $\left(\frac{dT}{dt}\right)_{\text{low}}$ for the phase-changing compounds in a) group 2, b) group 3, c) group 4, and d) group 5 of Table VI

droplet nuclei in case A, even if they do not by themselves reach a supersaturated state, is a result of the extended CNT for multicomponent aerosols, which assumes a group effect when forming the nuclei once at least one individual compound reaches its supersaturated state [1], [2]. The only compounds that are not present in the aerosol droplet nuclei are those, which have critical temperatures lower than the temperature the aerosol experiences.

As shown in Figs. 6 and 7, *glycerol* is the main constituent in the generated aerosol droplet nuclei in case A. This can also be observed in Fig. 8, where both the gas phase and liquid phase mass fractions are plotted together. For example, it can be seen that nearly all the gas phase Y_i undergoes a phase change to its liquid phase Z_i for *glycerol*, whereas only very small fractions of the gas phases are converted during the nucleation process for *nicotine* and *water*. This highlights the fact that *glycerol* is the major aerosol former in the EHTP under the assumed operating conditions and gas mixture composition. This is also supported by the saturation vapor pressure curves in Fig. 2, where *glycerol* has the lowest saturation vapor pressure at the temperatures considered.

It is important to remember that only the nucleation process is taken into account in this work and that the physical mechanisms of evaporation, condensation and coalescence are not included in the simulations presented here. These neglected mechanisms do not change the triggering of the nucleation process according to CNT and would only effect the evolution and the final composition of the already generated aerosol droplets [1].

The simulation results presented and discussed above indicate that according to the extended CNT for multicomponent aerosols, no aerosol droplets are formed from the minor compounds in Table VI as long as mainly *glycerol*, but also *nicotine* and *water* are not functioning as aerosol formers in the multicomponent gas mixture. To ensure that this conclusion is not sensitive to the amount of the minor compounds available in the gas mixture, simulations are performed where the initial masses of the minor compounds are increased from the values in case B by 50 times in case C, 100 times in case D, and 500 times in

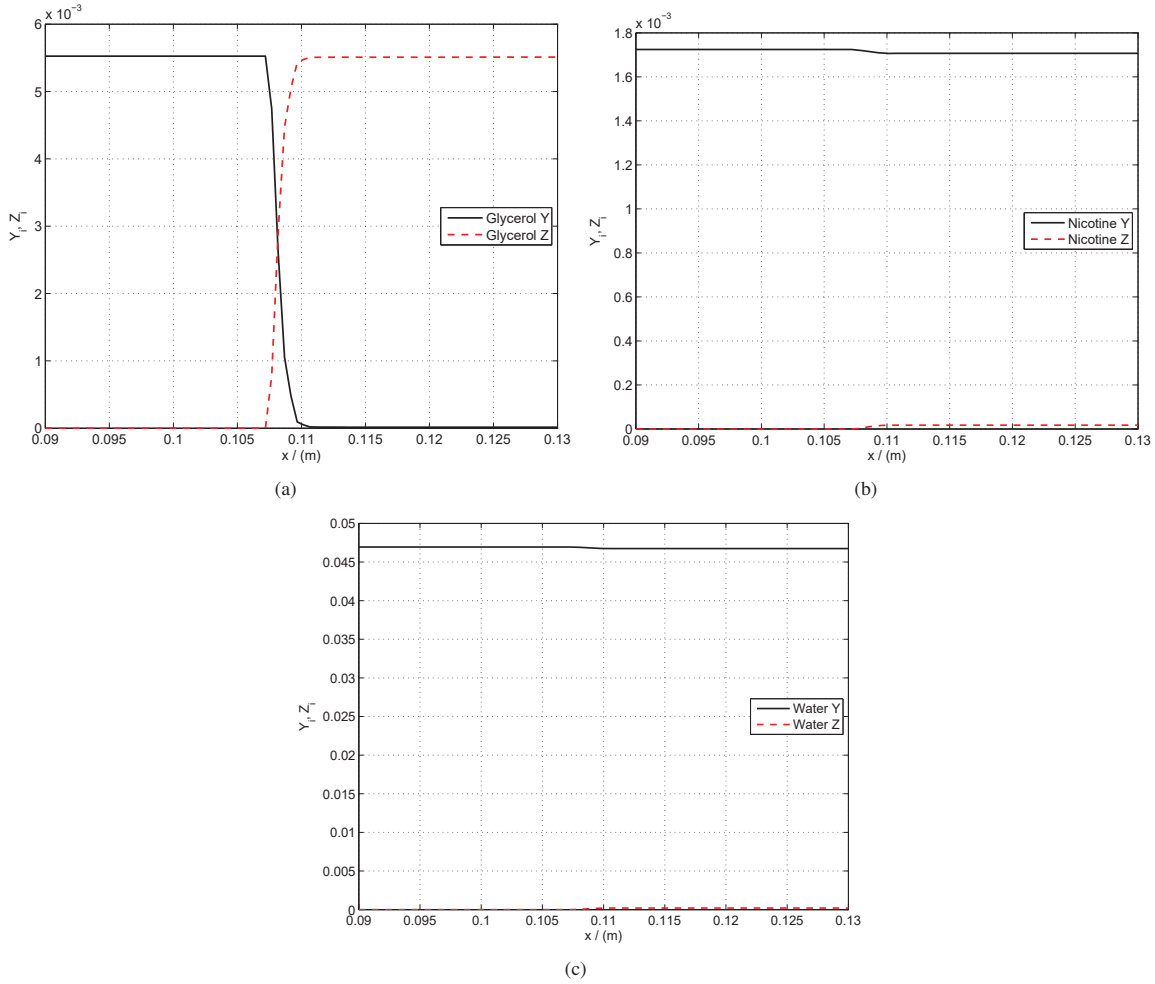

Fig. 8 Gas and liquid phase mass fractions along the x-axis (around the cooling region) at t_{end} for case A with $\left(\frac{dT}{dt}\right)_{\text{low}}$ for the phase-changing compounds a) *glycerol*, b) *nicotine*, and c) *water* in group 1 of Table VI

case E, as can be seen in Table V. The initial mass fractions for these cases are displayed in Table VI. As mentioned previously, case C represents a situation where the calculated total mass of compounds not identified nor quantified in the aerosol characterization carried out by Labstat International ULC are taken into account and represented by a 50-fold increase of the masses of the minor compounds tabulated in Table V. In the cases D and E, the amounts of the minor compounds largely surpass the reported values, representing situations where all minor compounds are released during a fraction of one puff of the HCI. It can be seen in Fig. 9 that aerosol droplets are not formed in either of the cases tested despite even a 500-fold increase of the amount of the minor compounds in the gas mixture in case E. This indicates that none of the minor compounds reach the supersaturated state necessary to trigger the nucleation process to form aerosol droplets. Given that even a 500-fold increase of the initial masses of the minor compounds does not trigger aerosol droplet formation according to the CNT, it can be concluded that it is the aerosol formers originating from evaporation that triggers the aerosol generation under the assumed gas mixture and operating conditions in the EHTP. This implies that even if all masses of the minor compounds collected and measured for an entire HCI protocol, cf. Table V, come in a single puff, they can according to the CNT not form aerosol droplets without the help of an aerosol former such as *glycerol*.

VI. Conclusion

In this work, aerosol formation in the EHTP during use when heated in the Holder (heating device) has been modeled using an extended CNT for multicomponent gas mixtures implemented into a FV-based CFD code for aerosol generation, transport and evolution [7]. The modeling approach aimed to investigate the aerosol formation characteristics for realistic heating operating conditions of the EHTP as well as for relevant gas mixture compositions of the EHTP aerosol experimentally measured. Results from

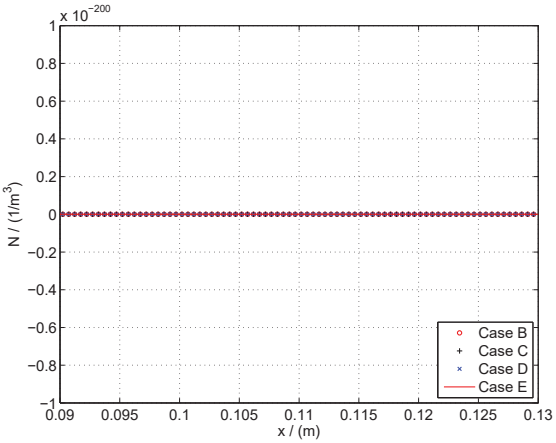

Fig. 9 Droplet number density along the x-axis (around the cooling region) at the time t_{end} for a) the case B, b) case C, c) case D, and d) case E of Table VI. For all cases the cooling rate is $\left(\frac{dT}{dt}\right)_{\text{low}}$

the performed simulations show that aerosol droplets are formed only in the presence of an aerosol former being mainly *glycerol* in this work. *Nicotine* and *water* were also shown to contribute to the generating of droplets under the test conditions. *Glycerol*, *nicotine* and *water* are evaporated from the tobacco plug when it is used as intended and heated by the Holder. Minor compounds of the gas mixture were shown to not be able to reach supersaturation alone and therefore could not generate aerosol droplets from the multicomponent gas mixture at the operating conditions simulated. For the measured gas mixture composition and estimated operating conditions of the tobacco plug in the EHTP, *glycerol* was demonstrated to be the aerosol former triggering the nucleation process in the EHTP. This implies that according to the extended CNT for multicomponent aerosols, an aerosol former, such as *glycerol* needs to be present in the gas mixture to form an aerosol under the tested operating conditions. To ensure that these conclusions are insensitive to the initial amount of the minor compounds tabulated in Table V and to represent the mass of compounds not analytically characterized in the studied performed by Labstat International ULC, simulations were carried out for which the initial masses of the minor compounds were increased by as much as a factor of 500. Despite this extreme condition, no aerosol droplet nuclei were formed when *glycerol*, *nicotine* and *water* were treated as inert species and therefore could not actively contribute to the nucleation process. This implies that according to the extended CNT for multicomponent aerosols, an aerosol cannot be generated from the minor compounds of the gas mixture alone at the compositions and operating conditions tested, i.e. representative of EHTP use conditions, even if all minor compounds, potentially generated via thermal decomposition reactions, are released or generated in a single puff.

Acknowledgment

All authors are employees of Philip Morris International. Philip Morris International is the sole source of funding and sponsor of this project. The authors would like to also thank E.M.A. Frederix and Prof. B.J. Geurts at University of Twente, The Netherlands, for their input and development of the aerosol model and algorithm.

References

[1] H. Vehkamäki, *Classical nucleation theory in multicomponent systems*. Springer-Verlag Berlin Heidelberg, 2006.
[2] W. Hinds, *Aerosol Technology*. New York: Wiley-Interscience, 1999.
[3] H. Nguyen, K. Okuyama, T. Mimura, Y. Kousaka, R. Flagan, and J. Seinfeld, "Homogeneous and heterogeneous nucleation in a laminar flow aerosol generator," *Journal of Colloid And Interface Science*, vol. 119, no. 2, pp. 491–504, 1987.
[4] M. Wilck, K. Hämeri, F. Stratmann, and M. Kulmala, "Experimental and theoretical examination of homogeneous nucleation in a laminar flow reactor (ucpc)," *Journal of Aerosol Science*, vol. 27, no. SUPPL.1, pp. S587–S588, 1996.
[5] M. P. Anisimov, E. G. Fominykh, S. V. Akimov, and P. K. Hopke, "Vapor-gas/liquid nucleation experiments: A review of the challenges," *Journal of Aerosol Science*, vol. 40, no. 9, pp. 733 – 746, 2009.
[6] C. Winkelmann, M. Nordlund, A. Kuczaj, S. Stolz, and B. Geurts, "Efficient second-order time-integration for single-species aerosol formation and evolution," *International Journal for Numerical Methods in Fluids*, vol. 74 (5), pp. 313–334, 2014.
[7] E. Frederix, M. Stanic, A. Kuczaj, M. Nordlund, and B. Geurts, "Extension of the compressible PISO algorithm to single-species aerosol formation and transport," *International Journal of Multiphase Flow*, vol. 74, pp. 184–194, 2015.
[8] H. Arstila, P. Korhonen, and M. Kulmala, "Ternary nucleation: Kinetics and application to water-ammonia-hydrochloric acid system," *Journal of Aerosol Science*, vol. 30, pp. 131–138, 1999.
[9] G. Wilemski, "Composition of the critical nucleus in multicomponent vapor nucleation," *The Journal of Chemical Physics*, vol. 80, no. 3, pp. 1370–1372, 1984.
[10] D. S. van Putten, "Efficient methods for N-component condensation," Ph.D. dissertation, University of Twente, Enschede, The Netherlands, 2011.
[11] R. Becker and W. Dring, "Kinetische behandlung der keimbildung in bersttigten dmpfen," *Annalen der Physik*, vol. 416, no. 8, pp. 719–752, 1935.
[12] "The OpenFOAM Foundation," http://www.openfoam.com, 2015.
[13] H. Jasak, "Error analysis and estimation for the finite volume method with applications to fluid flows," Ph.D. dissertation, Imperial College, University of London, 1996.
[14] M. Nordlund and A. Kuczaj, "Aerosol dosimetry modeling using computational fluid dynamics," in *Computational Systems Toxicology*, ser. Methods in Pharmacology and Toxicology, J. Hoeng and M. Peitsch, Eds. Humana Press: Springer, 2015.
[15] R. Bird, W. Stewart, and E. Lightfoot, *Transport Phenomena*, revised second ed. New York: John Wiley & Sons Inc., 2007.
[16] D. Kashchiev, *Nucleation: Basic Theory with Applications*. Butterworth-Heinemann: Elsevier Science, 2000.
[17] G. Wilemski and B. E. Wyslouzil, "Binary nucleation kinetics. I. Self-consistent size distribution," *The Journal of Chemical Physics*, vol. 103, no. 3, pp. 1127–1136, 1995.
[18] D. S. van Putten, S. P. Glazenborg, R. Hagmeijer, and C. H. Venner, "A multigrid method for N-component nucleation," *The Journal of Chemical Physics*, vol. 135, no. 1, 2011.
[19] R. Issa, B. Ahmadi-Befrui, K. Beshay, and A. Gosman, "Solution of the implicitly discretised reacting flow equations by operator-splitting," *Journal of Computational Physics*, vol. 93, pp. 388–410, 1991.
[20] R. Baker, "The development and significance of standards for smoking-machine methodology," *Beitrge zur Tabakforschung / Contributions to Tobacco Research*, vol. 20, no. 1, pp. 23–41, 2002.
[21] "Philip Morris International," http://www.pmiscience.com, 2016.
[22] F. Barontini, A. Tugnoli, V. Cozzani, J. Tetteh, M. Jarriault, and I. Zinovik, "Volatile products formed in the thermal decomposition of a tobacco substrate," *Industrial & Engineering Chemistry Research*, vol. 52, no. 42, pp. 14 984–14 997, 2013.

[23] V.-G. V. und Chemieingenieurwesen and V. Gesellschaft, *VDI Heat Atlas*, ser. Springer reference. Springer, 2010.
[24] "CAMEO Chemicals database," http://cameochemicals.noaa.gov, 2015.
[25] T. Daubert, R. Danner, and N. Design Institute for Physical Property Data (New York, *Data compilation tables of properties of pure compounds*. American Institute of Chemical Engineers, 1985, no. Teil 2.
[26] B. Poling, J. Prausnitz, and J. O'Connell, *The properties of gases and liquids*. McGraw-Hill, 2001.
[27] R. Warming and R. Beam, "Upwind second-order difference schemes and applications in aerodynamic flows," *AIAA Journal*, vol. 14, pp. 1241–1249, 1976.